Applied Catalysis B: Environmental 300 (2022) 120713

Contents lists available at ScienceDirect

Applied Catalysis B: Environmental

journal homepage: www.elsevier.com/locate/apcatb

FeMn@HZSM-5 capsule catalyst for light olefins direct synthesis via Fischer-Tropsch synthesis: Studies on depressing the CO_2 formation

Faen Song [a], Xiaojing Yong [c], Xuemei Wu [a], Wei Zhang [c], Qingxiang Ma [b], Tiejian Zhao [c], Minghui Tan [a,*], Zhongshan Guo [c], Heng Zhao [d], Guohui Yang [a,*], Noritatsu Tsubaki [d,*], Yisheng Tan [a]

[a] State Key Laboratory of Coal Conversion, Institute of Coal Chemistry, Chinese Academy of Sciences, Taiyuan 030001, China
[b] State Key Laboratory of High-efficiency Coal Utilization and Green Chemical Engineering, Ningxia University, Yinchuan 750021, China
[c] National Energy Group Ningxia Coal Industry Co., Ltd., Yinchuan, China
[d] Department of Applied Chemistry, School of Engineering, University of Toyama, Toyama 930-8555, Japan

ARTICLE INFO

Keywords:
Fischer-Tropsch synthesis
Water-gas shift reaction
FeMn catalyst
Capsule catalyst
Core-shell structure

ABSTRACT

For Fe-based Fischer-Tropsch synthesis catalyst, how to decrease CO_2 formation is a big challenge. In this work, a capsule catalyst (FeMn@HZSM-5) with FeMn as core and HZSM-5 as shell was prepared and used for Fischer-Tropsch to olefins (FTO) reaction, compared with bare FeMn catalyst and several hybrid catalysts by physically mixing FeMn and HZSM-5 in different ways. Among these catalysts, the FeMn@HZSM-5 capsule catalyst showed the best catalytic performance with the highest light olefins selectivity and the lowest CO_2 selectivity. Compared with FeMn catalyst, the CO_2 selectivity of FeMn@HZSM-5 catalyst decreased more than 10%. However, the CO_2 selectivity of other physically mixing catalysts was similar to that of bare FeMn catalyst, indicating that randomly adding HZSM-5 had no effect on depressing the CO_2 formation. Benefiting from the HZSM-5 shell, the FeMn@HZSM-5 capsule catalyst could effectively affect the diffusion of H_2O and thus suppress the water-gas shift reaction in FTO reaction.

1. Introduction

Light olefins (C_2–C_4 olefins) are important building blocks for chemical industry, traditionally produced by cracking of naphtha or obtained as byproducts from oil refining processes [1]. With the depletion of petroleum resource, developing alternative non-oil routes is urgently needed. Coal, natural gas or biomass are promising alternative feed stocks to produce light olefins via syngas (a mixture of CO and H_2) as intermediate platform. Recently, many significant advancements in direct and highly selective synthesis of light olefins from syngas have been made by Fischer-Tropsch to olefins (FTO) process and oxide-zeolite (OX-ZEO) process, respectively [2–10]. As a promising process with higher one-pass conversion, FTO process has attracted extensive attentions [11–17].

Many catalytic systems based on different metallic catalysts, such as iron, cobalt, and ruthenium, have been studied for Fischer-Tropsch synthesis (FTs). Most researches are focused on Fe-based or Co-based catalysts in FTO process because of their low cost, high activity and good stability [6,18–24]. In comparison to Co, Fe with the lower hydrogenation ability is unbeneficial for the secondary hydrogenation reactions of olefins and readily reaches higher selectivity of olefins. Therefore, Fe-based catalysts exhibit more promising prospect for the future industrial application for FTO [18,25–29]. The main goals of FTO are to increase the selectivity of lower olefins, reduce the production of methane, and avoid the formation of excessive CO_2 [11,30–32]. Although many efforts have been devoted to FTO, developing a catalyst to achieve all aims is a great challenge. Limited by the Anderson–Schulz–Flory (ASF) production distribution of FTs, increasing the selectivity of lower olefins always leads to the high production of methane [11]. In comparison to other FTO catalysts, Fe-based catalyst could realize high selectivity of light olefins with lower methane production. Especially when the manganese is used as the promoter for Fe-based catalysts, the formation of methane is suppressed and the selectivity of light olefins is enhanced effectively [13,33–37]. Moreover, the addition of sodium and sulfur promoters can further suppress the formation of methane to increase the selectivity of light olefins [38–41].

* Corresponding authors.
E-mail addresses: tanmh@sxicc.ac.cn (M. Tan), yanggh@sxicc.ac.cn (G. Yang), tsubaki@eng.u-toyama.ac (N. Tsubaki).

https://doi.org/10.1016/j.apcatb.2021.120713
Received 27 June 2021; Received in revised form 4 September 2021; Accepted 8 September 2021
Available online 13 September 2021

However, Fe-based catalysts possess high water-gas shift (WGS) reaction activity, thus yield the high selectivity of CO_2 [11,42]. Although the high WGS reaction activity of Fe-based catalysts is beneficial to adjust the H_2/CO ratio for the CO-rich syngas, it is undesired for syngas with suitable H_2/CO ratio. Moreover, the excessive formation of CO_2 results in lower utilization ratio of carbon resource and will intensify the greenhouse effect. Although abundant works for FTO are focused on the investigation of active metals or promoters, the effect of catalyst on suppressing the WGS reaction is almost ignored. Therefore, how to avoid the WGS reaction for Fe-based catalyst to further achieve higher selectivity of light olefins is deserved to be studied. In order to simultaneously achieve high selectivity of lower olefins and low methane selectivity, as well as low CO_2 selectivity, development of novel FTO catalysts is necessary and important.

As a kind of effective FTs catalyst, capsule catalysts with special core-shell structure have showed excellent catalytic performance for FTs in past studies [43–47]. These capsule catalysts, usually composed of FTs catalysts as core and acidic zeolites as shell, could break the ASF production distribution and realize high selectivity of target products by the synergistic confinement effect between core and shell catalysts. Through the design and optimization of the core and shell materials, the capsule catalyst could realize bifunctional catalysis and its catalytic performance was always better than that of the corresponding physical mixture catalyst [48,49]. Recently, a core-shell structured Zn-Cr@SAPO capsule catalyst fabricated from a physical encapsulation method exhibited a unique strategy to advance the light olefin selectivity and limit CO_2 formation in OX-ZEO process [50].

In this study, a FeMn@HZSM-5 capsule catalyst with core-shell structure was prepared and used for FTO reaction. Compared with bare FeMn catalyst, the capsule catalyst could effectively depress the formation of CO_2 and thus reduce CO_2 selectivity. In order to investigate the role of the core-shell structure and HZSM-5 shell of FeMn@HZSM-5, several physically mixed catalysts with different mixing mode were also tested at the same conditions. The decreasing of CO_2 selectivity was only obtained by the FeMn@HZSM-5 capsule catalyst. Otherwise, both the shell thickness and Si/Al ratio of zeolite shell exerted promotional function in suppressing the CO_2 formation and increasing the hydrocarbon selectivity consequently.

2. Experimental

2.1. Materials

All chemicals were commercially available and used without any further purification.Ferric nitrate ($Fe(NO_3)_3{\cdot}9H_2O$, 98%), manganese nitrate ($Mn(NO_3)_2{\cdot}6H_2O$, 99%), potassium carbonate (K_2CO_3, 99%) and silica sol (30 wt% SiO_2 in water) were purchased from Sigma-Aldrich. HZSM-5 zeolites with different Si/Al ratio were purchased from Nankai University Catalyst Co., Ltd.

2.2. Catalyst preparation

2.2.1. FeMn catalyst

The FeMn catalyst was prepared by the co-precipitation method. An aqueous solution containing ferric nitrate and manganese nitrate (Fe/Mn molar ratio = 10/1) was added into a beaker containing some deionized water with vigorous stirring, while another aqueous solution of K_2CO_3 as precipitant was simultaneously added into the beaker to form a suspension liquid and kept the pH value at 8.0. The co-precipitation was carried out at 60 °C and subsequently the precipitate was aged for 2 h under stirring at the same temperature. After filtration and washing, the catalyst was dried at 110 °C for 12 h and calcined at 400 °C for 4 h. Before reaction, the FeMn catalyst was granulated with the size of 0.85–1.70 mm.

2.2.2. FeMn@HZSM-5 capsule catalyst

The FeMn@HZSM-5 catalyst with FeMn as core and HZSM-5 as shell was prepared by a simple cladding method. The detailed preparation procedures were as followed: A certain amount of silica sol (30 wt%) was diluted with 2 times deionized water in weight. The diluted silica sol, as a binder, was used to moisten the granulated FeMn catalyst. And then HZSM-5 (SiO_2/Al_2O_3 = 38) powder was mixed with the soaked FeMn catalyst in a round bottomed flask by simple manual stirring. The weight ratio of FeMn to HZSM-5 was 3/1. The obtained sample was finally treated by calcination at 400 °C for 4 h.

2.2.3. FeMn/HZSM-5 catalyst

The FeMn/HZSM-5 catalyst with 3/1 wt ratio of FeMn and HZSM-5 (SiO_2/Al_2O_3 = 38) powders was prepared by a mechanically mixing method. After homogeneously mixing of FeMn and HZSM-5 powder, the mixture was shaped to the same size with granulated FeMn catalyst.

2.2.4. FeMn^HZSM-5 catalyst

The FeMn^HZSM-5 catalyst was obtained by crushing FeMn@ZSM-5 capsule catalyst to powder, then granulating the powder again.

2.2.5. FeMn&HZSM-5 catalyst

The FeMn&HZSM-5 catalyst was obtained by mixing the granulated FeMn catalyst and granulated HZSM-5.

2.2.6. FeMn%HZSM-5 catalyst

The FeMn%HZSM-5 catalyst was obtained by mixing the granulated FeMn catalyst and HZSM-5 powder.

2.2.7. FeMn/SiO_2 catalyst

FeMn/SiO_2 catalyst was prepared by moistening the granulated FeMn catalyst with diluted silica sol. The amount of diluted silica sol used was the same as the preparation process of FeMn@HZSM-5 catalyst. Then the sample was dried and calcined in air at 400 °C for 4 h.

2.3. Catalyst characterization

The X-ray diffraction (XRD) analysis was carried out on a Bruker Advanced X-Ray Solutions/D8-Advance using Cu Kα radiation. The surface morphology and element composition were detected by scanning electron microscopy (SEM) (JSM-7001F, JEOL, Japan) with energy dispersive X-ray spectroscopy (EDS). The BET specific surface areas of catalysts were calculated by N_2 adsorption/desorption isotherm obtained from a physisorption analyzer (ASAP 2020, Micromeritics Instrument Corporation, USA). The H_2 temperature-program reduction (H_2-TPR) was used to analyze the reduction property of catalysts on a temperature programmed adsorption instrument (TP-5080, Tianjin Xianquan Corporation, China). The CO_2 temperature-programed desorption (CO_2-TPD) with a heating rate of 5 °C/min was performed on the same apparatus with H_2-TPR.

The temperature program surface reaction (TPSR) and WGS reaction were carried out on a micro-reactor equipped with a mass analyzer (MS, OMNISTAR). The typical TPSR process is following: 0.1 g FeMn catalyst or 0.133 g hybrid catalysts was put in the quartz tube to keep same loading of FeMn core catalyst and reduced by 10%H_2/Ar (30 mL/min) at 300 °C for 2 h. After reduction, the gas was switched to Ar at 300 °C until the temperature decreasing to 50 °C. Then, the gas was switched to syngas (CO/H_2 = 1/2) and the temperature was increased from 50 to 500 °C with a heating ramp of 10 °C/min. The reaction tail gas was collected and analyzed by MS. For WGS reaction, after reduction, the gas was switched to Ar and the temperature decreased to 280 °C and kept for 2 h. Then the gas was switched to CO and water vapor keeping the temperature at 280 °C, and the mass spectrum began to record the reaction tail gas simultaneously and immediately.

2.4. Catalytic test

Catalyst activity test of various catalysts for FTO reaction was carried out in a continuous flow type fixed-bed reactor system. 2 mL catalyst (30–50 mesh) was packed into the reactor made with stainless steel. Prior to test, all catalysts were heated to 300 °C with a heating ramp of 2 °C/min and in-situ reduced by 10%H_2/N_2 at 300 °C for 4 h under atmospheric pressure. Then, feed gas ($H_2/CO = 2/1$, containing 3%N_2 as inner standard) was fed into the reactor and the reactions were performed at 280 °C and 1 MPa, with a gas hourly space velocity (GHSV) of 2000 h^{-1}. The gaseous product was analyzed by an online gas chromatography (GC-2010, Shimadzu) equipped with a thermal conductivity detector (TCD) and an online gas chromatography (GC-2014, Shimadzu) equipped with a flame ionization detector (FID). The liquid product was collected, weighed and analyzed by an offline gas chromatography (GC-2014, Shimadzu) equipped with a flame ionization detector (FID). The CO conversion was calculated according to the following equation:

$$\text{CO Conversion} = \frac{CO_{inlet}\text{-}CO_{outlet}}{CO_{inlet}} \times 100\%$$

Where CO_{inlet} and CO_{outlet} represent moles of CO at the inlet and outlet, respectively.

The product selectivity was calculated by the following equation:

$$\text{Product Selectivity} = \frac{C_x}{\sum C_x} \times 100\%$$

Where C_x represents the carbon mole of product x at the outlet, respectively. The carbon balance of all reactions in this article is in the range of 100 ± 5%.

3. Results and discussion

3.1. Structure characterization of catalysts

Fig. 1 exhibits the XRD patterns of FeMn, HZSM-5, FeMn@HZSM-5 and FeMn/HZSM-5 catalysts. These peaks at 24.2, 33.1, 35.6, 40.8, 49.5, 54.0, 57.6, 62.5 and 64.0°on FeMn can be attributed to the (012), (104), (110), (113), (024), (116), (018), (214) and (300) planes of α-Fe_2O_3 (JCPDS no. 33-0664). For the direct physically mixed FeMn/HSM-5 catalyst, some typical diffraction peaks of HZSM-5 at 5–30° appear due to the addition of HZSM-5. Similar to the FeMn/HSM-5 catalyst, the FeMn@HZSM-5 catalyst also shows these peaks of the HZSM-5. It indicates that the HZSM-5 crystals are successfully coated on FeMn core by the cladding method for zeolite shell preparation.

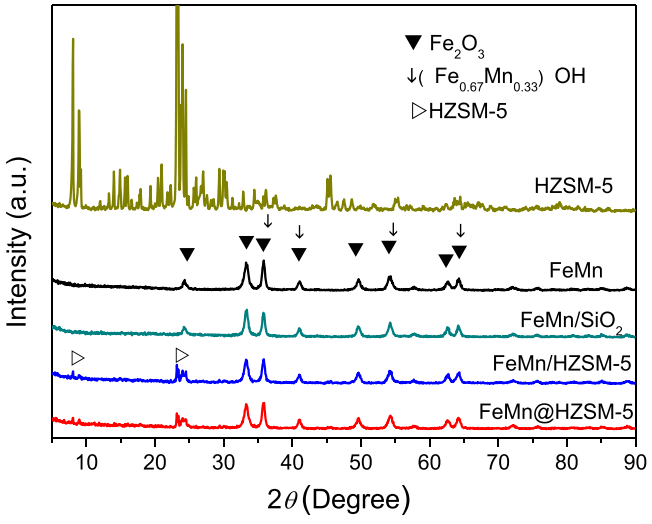

Fig. 1. XRD patterns of FeMn, HZSM-5 and hybrid catalysts.

The surface morphology and element composition of FeMn and FeMn@HZSM-5 catalysts can be analyzed by SEM-EDS. As shown in Fig. 2(a) and (b), the surface of FeMn is smooth and the Fe/Mn ratio is close to 10/1. In comparison to FeMn catalyst, the surface of FeMn@HZSM-5 is coarse and homogeneously coated by the HZSM-5 zeolite crystals (Fig. 2(c) and inset in (c)), which also indicates the successful formation of HZSM-5 shell on the FeMn core catalyst. Moreover, the surface element signals of FeMn@HZSM-5 obtained by EDS (Fig. 2d) only have Si, Al and O, while no Fe or Mn signal is detected. The result suggests that the FeMn core catalyst is completely and compactly covered by HZSM-5 and the FeMn@HZSM-5 capsule catalyst has an integrated core-shell structure. Fig. 2(e) and (f) show the cross-section SEM image and EDS line analysis results of FeMn@HZSM-5 capsule catalyst, respectively. As shown in the inset of Fig. 2(e), the whole FeMn core catalyst has been enwrapped by HZSM-5 zeolite crystals completely and the thickness of zeolite shell is in range of 15–40 μm. The corresponding EDS line analysis of element signals (Fig. 2(f)) along the red line in Fig. 2(e) exhibits the decrease of Si signal and the increase of Fe signal from the zeolite shell to the core.

The specific surface areas (SSA) of these catalysts were obtained by N_2 adsorption/desorption isotherms as shown in Fig. 3. The SSA of FeMn core catalyst is 75.3 m^2/g, while that of FeMn@HZSM-5 capsule catalyst increases to 115.4 m^2/g due to the addition of HZSM-5 shell.

Hydrogen temperature-programmed reduction (H_2-TPR) was used to characterize the reduction property of FeMn catalyst and hybrid catalysts in Fig. 4. All catalysts exhibit three peaks at 300, 400 and 630 °C, which can be assigned to the reduction of Fe species: Fe_2O_3 to Fe_3O_4, Fe_3O_4 to FeO and FeO to Fe, respectively [40]. Compared with bare FeMn catalyst, there exists almost no difference in the temperature of all reduction peaks for these hybrid catalysts. The result indicates that the addition of HZSM-5 does not influence the reduction property of FeMn due to the negligible interaction between FeMn and HZSM-5.

3.2. Catalytic performance for FTO reaction

FeMn catalyst and various hybrid catalysts were tested for FTO reaction. To investigate the effect of the HZSM-5 shell, or adding HZSM-5 by other ways, on the catalytic performance of FeMn for FTO, the catalytic activity and products selectivity of these catalysts are listed in Table 1. For the bare FeMn catalyst, although it has the high CO conversion of 83.8% and low CH_4 selectivity of 17.0%, high CO_2 selectivity of 39.4% is also obtained, which accords with the catalytic property of Fe-based FTs catalysts (Table S1). In comparison to bare FeMn catalyst, the CO conversion over FeMn@HZSM-5 capsule catalyst presents a slight decrease from 83.8% to 78.5%, due to the coverage of HZSM-5 shell. Nevertheless, for the FeMn@HZSM-5 capsule catalyst, the selectivity of CO_2 decreases more than 10% (to 28.3%). The result suggests the WGS reaction could be suppressed to decrease the CO_2 formation by building the HZSM-5 shell of capsule catalyst. Therefore, more CO could be converted to hydrocarbon and the selectivity of hydrocarbon (CH_n) increases from 59.1% to 70.0%. Consequently, the carbon utilization ratio could be effectively improved by suppressing the WGS reaction. In comparison with some other FeMn based catalysts (Table S1), the FeMn@HZSM-5 capsule catalyst also exhibits lower CO_2 selectivity with high CO conversion and hydrocarbon selectivity. On the other hand, due to its hydrocracking function, the HZSM-5 shell also contributes to depress the formation of higher carbon hydrocarbon and the selectivity of C_5^+ over FeMn@HZSM-5 capsule catalyst is lower than that over FeMn catalyst.

As reference catalysts, several physical mixture catalysts with different mixing ways were also performed the FTO reactions under the same reaction conditions. Unfortunately, although adding HZSM-5, the CO_2 selectivity over these physical mixture catalysts does not present the obvious decrease as FeMn@HZSM-5 capsule catalyst. The influence of the mixture ways between FeMn and HZSM-5 on the catalytic

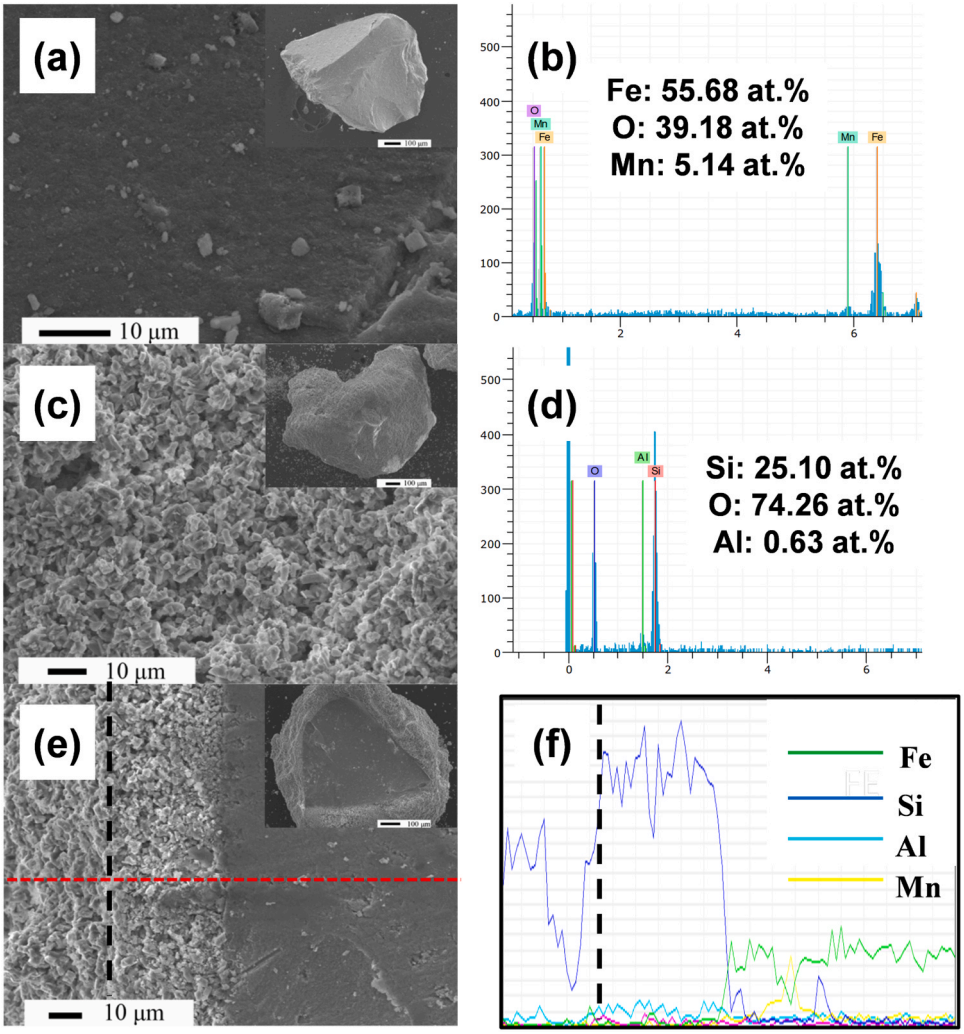

Fig. 2. SEM-EDS of FeMn and FeMn@HZSM-5 catalysts: (a) Surface SEM image and (b) EDS analysis of FeMn; (c) Surface SEM image and (d) EDS analysis of FeMn@HZSM-5; (e) cross-section SEM image and (f) EDS line analysis of FeMn@HZSM-5. Scale bars in insets of (a, b, c) represent 100 μm.

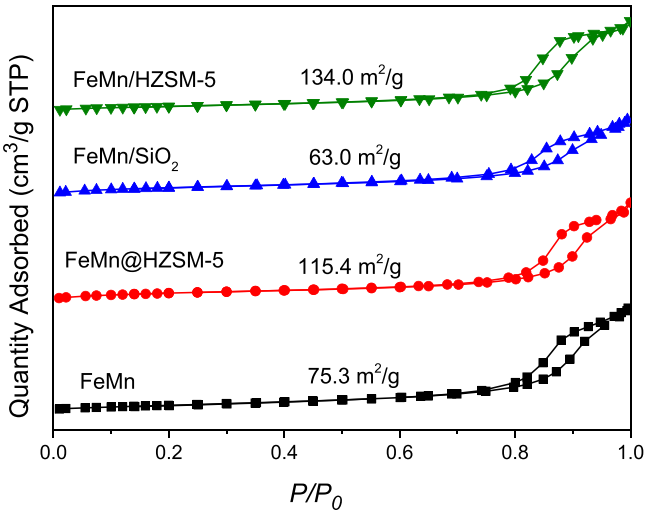

Fig. 3. N_2 adsorption/desorption isotherms of FeMn catalyst and hybrid catalysts.

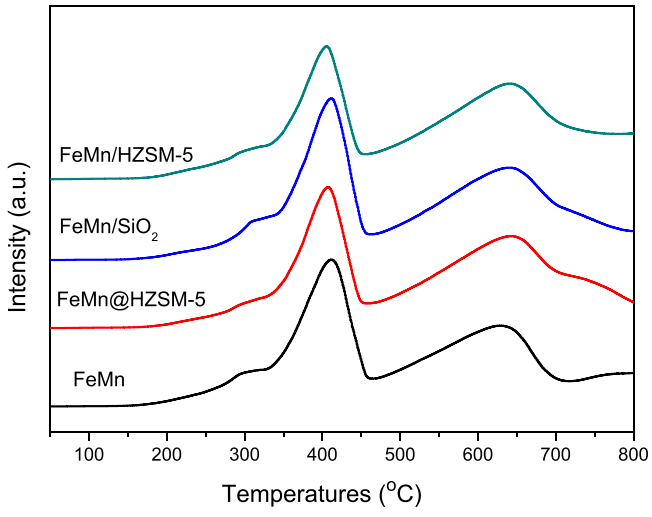

Fig. 4. H_2-TPR of FeMn catalyst and hybrid catalysts.

performance can be compared more clearly in Fig. 5. Although the hydrocarbon selectivity increases slightly and the CO_2 selectivity decreases slightly over these physically mixing catalysts, the significantly

Table 1
Catalytic activity and product selectivity of various catalysts.

Catalyst	CO Conv. (%)	Selec. (Cmol%)			Hydrocarbon distribution (wt%)								
		CH_n	CO_2	Oxy	C_1	C_2	$C_2^=$	C_3	$C_3^=$	C_4	$C_4^=$	C_5^+	($C_{2-4}^=$)
FeMn	83.8	59.1	39.4	1.5	17.0	8.1	6.1	3.3	17.7	2.8	13.6	31.4	37.5
FeMn@HZSM-5	78.5	70.0	28.3	1.8	18.7	9.1	7.3	4.1	19.1	3.0	14.9	23.8	41.4
FeMn/HZSM-5	82.2	63.9	35.5	0.6	20.2	11.4	6.8	5.1	17.5	2.9	14.0	22.3	38.2
FeMn^HZSM-5	86.4	63.5	35.2	1.2	20.0	11.6	5.2	5.5	17.1	3.1	14.8	22.6	37.1
FeMn&HZSM-5	83.1	62.0	37.2	0.8	15.8	10.0	6.4	4.7	15.8	3.0	15.4	29.0	37.6
$FeMn/SiO_2$	83.6	61.0	37.4	1.6	16.1	7.4	7.0	3.2	18.0	2.8	13.6	32.0	38.5

Reaction conditions: 2 mL of catalyst, 280 °C, 1 MPa, $H_2/CO = 2$, TOS = 12 h, and GHSV = 2000 h^{-1}, CH_n means all hydrocarbons, Oxy means DME and alcohols.

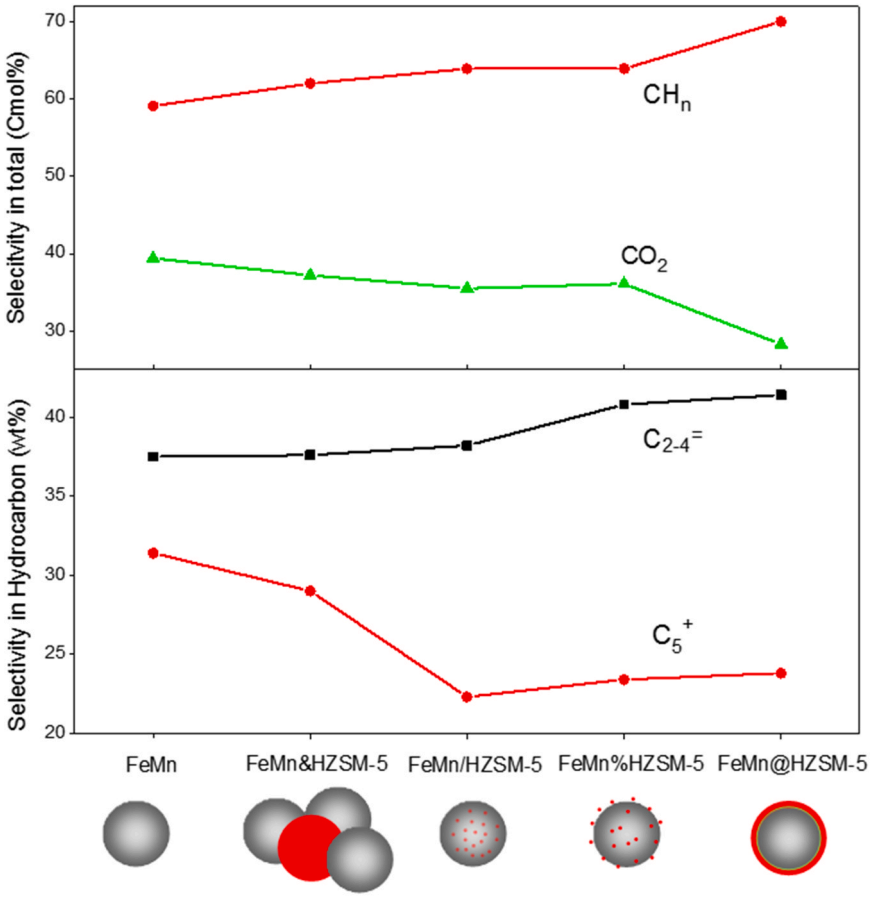

Fig. 5. FTO performance over FeMn and hybrid catalysts with different mixture ways between FeMn catalyst and HZSM-5.

improved catalytic performance is only obtained by the capsule catalyst. This interesting result indicates that suppressing the WGS reaction does not depend on randomly adding HZSM-5, but depends on the specific core-shell structure of the FeMn@HZSM-5 capsule catalyst.

3.3. *Influence of core-shell structure on the WGS reaction*

The influence of FeMn@HZSM-5 capsule catalyst on the WGS reaction in FTO can be confirmed by temperature program surface reaction (TPSR). Fig. 6 presents the signals of CO ($m/z = 28$), CH_4 ($m/z = 16$), H_2O ($m/z = 18$) and CO_2 ($m/z = 44$) from TPSR data of FeMn, FeMn@HZSM-5, and FeMn/HZSM-5 catalysts. As shown in Fig. 6(a), the CO signals of all catalysts exhibit the similar trend and decrease with the increasing temperature. This is because that higher temperature (especially higher than 300 °C) can promote the conversion of CO to produce hydrocarbon, water (from FTO reaction) and CO_2 (from WGS reaction). Therefore, the CH_4 signals of all catalysts increase with the temperature as in Fig. 6(b). However, an interesting result is obtained about the change of H_2O signals for three catalysts as in Fig. 6(c). With the hydrogenation of CO (Fig. 6(a)) and production of hydrocarbon (Fig. 6(b)), more water will also be produced. Whereas, for FeMn and FeMn/HZSM-5 catalysts, the H_2O signals exhibit a decrease trend (Fig. 6(c)). The decrease of H_2O can be attributed to the H_2O consumption of WGS reaction, indicating that the WGS reaction on FeMn and FeMn/HZSM-5 catalysts happens readily and rapidly. But for FeMn@HZSM-5 capsule catalyst, the H_2O signal does not decrease, but increases slightly. It indicates that the produced H_2O on FeMn@HZSM-5 capsule catalyst almost does not take part in the WGS reaction and is not consumed rapidly, unlike those on FeMn and FeMn/HZSM-5 catalysts. As a result, the CO_2 signal of FeMn@HZSM-5 increases more slowly than those of FeMn and FeMn/HZSM-5 catalysts, as compared in Fig. 6(d). This result suggests that benefiting from the HZSM-5 shell, the produced water cannot readily reach the active site on FeMn core catalyst and the WGS reaction on FeMn@HZSM-5 catalyst is suppressed effectively. The existence of HZSM-5 shell inhibits the mutual diffusion of H_2O between FeMn core catalysts, which reduces the utilization of active sites for WGS

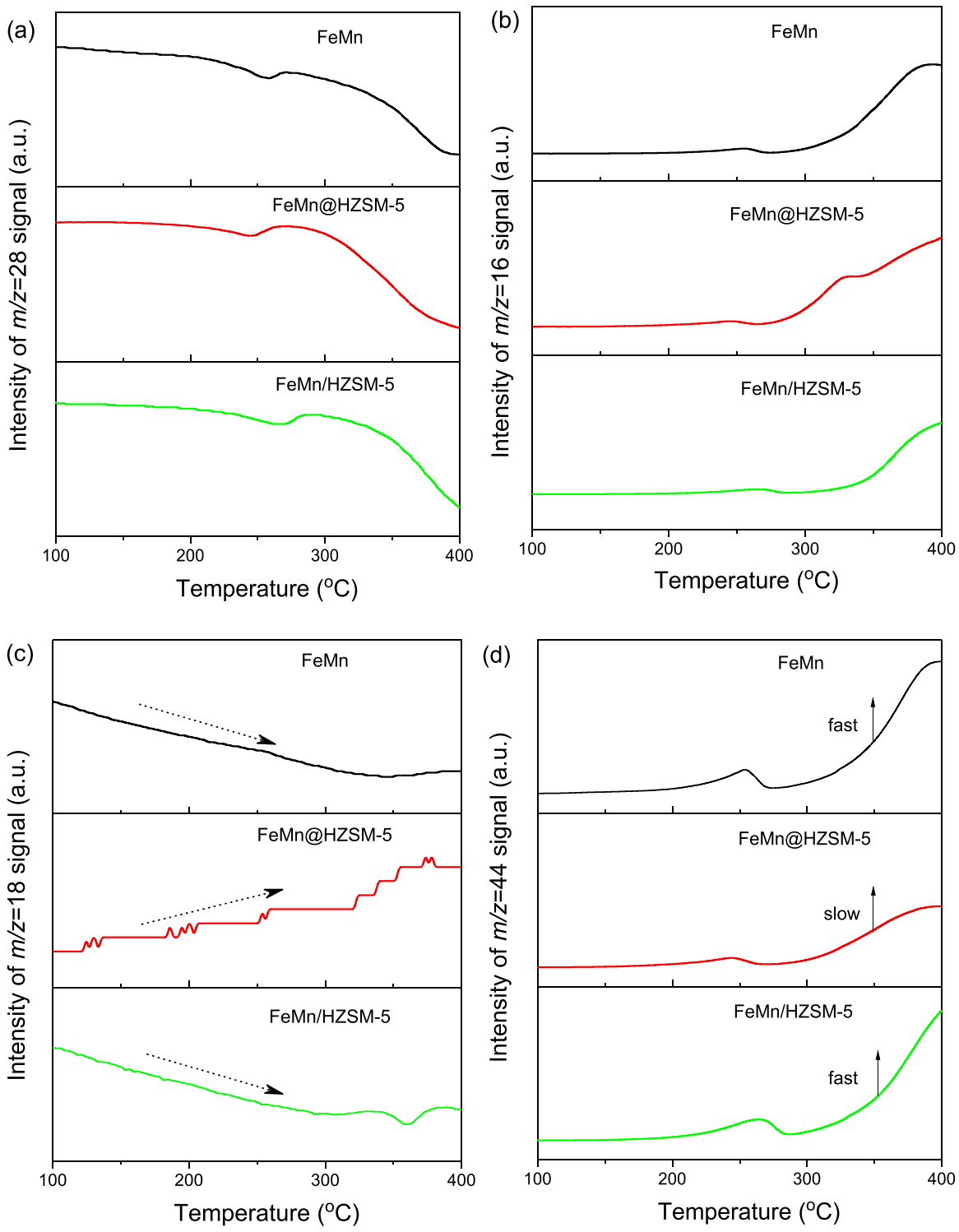

Fig. 6. TPSR of FeMn, FeMn@HZSM-5 and FeMn/HZSM-5 catalyst: (a) $m/z = 28$ signal; (b) $m/z = 16$ signal; (c) $m/z = 18$ signal; (d) $m/z = 44$ signal.

reaction and thus lowered the happening probability of the WGS reaction.

To further investigate the effect of core-shell structure of FeMn@HZSM-5 capsule catalyst on the diffusion of H_2O and WGS reaction, a self-designed WGS reaction was operated to investigate the difference between FeMn and FeMn@HZSM-5. When a gas flow containing CO and water vapor was injected into the tube reactor loaded with pre-reduced FeMn or FeMn@HZSM-5 catalyst at 280 °C, the mass spectrum began to record the reaction tail gas immediately and the signal of $m/z = 44$ (CO_2) was chosen to monitor the WGS reaction status. As shown in Fig. 7, for bare FeMn catalyst, the signal of CO_2 begins to increase earlier and arises much more quickly than FeMn@HZSM-5 capsule catalyst. It manifests that the HZSM-5 shell of the capsule catalyst can efficiently depress H_2O diffusion to the FeMn core catalyst (including neighboring FeMn cores) and thus lower the reaction rate of WGS reaction. Moreover, the integral area of FeMn@HZSM-5 capsule catalyst is obviously smaller than that of FeMn, indicating the lower WGS reaction activity of the capsule catalyst. Otherwise, in comparison

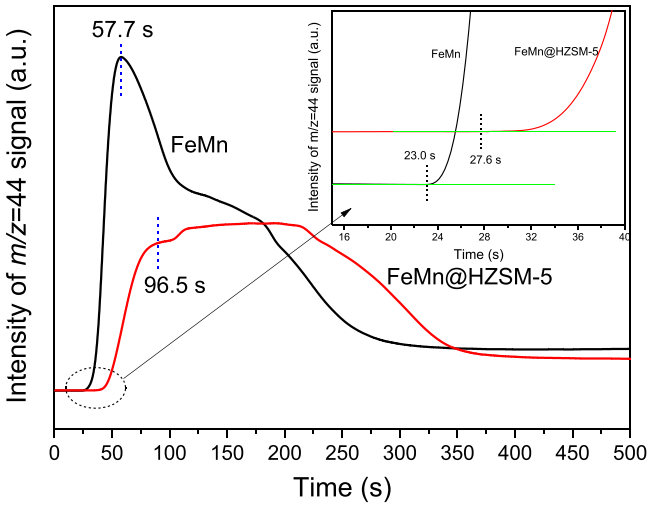

Fig. 7. The CO_2 signal vs. time of WGS reaction for FeMn and FeMn@HZSM-5 catalysts. The temperature was kept at 280 °C.

to FeMn@HZSM-5 catalyst, the signal intensity of FeMn catalyst peaks begins to fall quickly, suggesting that the FeMn catalyst owns high initial WGS reaction activity but decreases more quickly. However, the HZSM-5 shell of the capsule catalyst can lower the WGS reaction activity being accompanied by a slightly decreasing trend. These results obtained from TPSR and WGS reaction both prove that the special core-shell structure of FeMn@HZSM-5 capsule catalyst can suppress the H_2O diffusion and the WGS reaction activity. Otherwise, the addition of HZSM-5 could also affect the CO_2 desorption and diffusion. As evidenced by CO_2-TPD curves in Fig. S1, in comparison to bare FeMn catalyst, the second desorption peaks of FeMn@HZSM-5 and FeMn/HZSM-5 shift to higher temperature, which indicates that HZSM-5 can depress the CO_2 desorption and diffusion. For FeMn@HZSM-5 catalyst, being assisted by the confined space realized by HZSM-5 shell, more CO_2 will accumulate in the shell, thus further suppress the WGS reaction activity of FeMn core catalyst.

3.4. *Influence of the shell thickness and Si/Al ratios of HZSM-5*

The above result discloses that the special core-shell structure of FeMn@HZSM-5 capsule catalyst plays an important role in the suppression of WGS reaction and CO_2 production. Therefore, the shell thickness of HZSM-5 should be a key factor to affect the water diffusion and WGS reaction. Thus, FeMn@HZSM-5 capsule catalysts with different shell thickness were prepared by adopting varied HZSM-5/FeMn mass ratios. Fig. 8 compares the catalytic performance of these catalysts to the bare FeMn catalyst. In comparison to FeMn catalyst, the FeMn@HZSM-5 capsule catalyst with low HZSM-5/FeMn mass ratio (1/6) has exhibited effective effect on inhibiting CO_2 production and promoting hydrocarbon selectivity. With the increase of HZSM-5/FeMn mass ratios from 1/6 to 1/3, the CO_2 selectivity decreases and the hydrocarbon selectivity increases to some extent, respectively. However, further increasing the ratio from 1/3 to 1/2, the CO_2 selectivity and hydrocarbon selectivity are almost unchanged, and higher mass ratios (1/3 and 1/2) lead to some decrease of CO conversion. It may be attributed to the fact that H_2O diffusion achieves the equilibrium, thus further increasing thickness cannot always decrease the CO_2 formation. The result indicates that appropriate thickness of zeolite shell is beneficial for depressing the CO_2 formation. Increasing the thickness of zeolite shell can hinder the H_2O diffusion into core and thereby decrease the WGS reaction rate, suppressing CO_2 formation.

Besides the thickness of zeolite shell, the properties of zeolite are also important factors, such as the Si/Al ratio. Different Si/Al ratio can change the acidic sites and surface chemical property. Fig. S2 exhibited the NH_3-TPD of FeMn@HZSM-5 catalysts with different Si/Al ratios of HZSM-5 zeolite. With the increasing Si/Al ratio, both weak acid and strong acid decreased gradually. Due to the change of acidic property, the Si/Al ratio can tune surface hydrophobicity of zeolite, which can affect the adsorption and diffusion of H_2O in zeolite. For the FeMn@HZSM-5 capsule catalyst, the produced H_2O on FeMn core catalyst will diffuse through the HZSM-5 shell and the ZSM-5 shell can hinder the diffusion of this H_2O and change the concentration of H_2O in shell, which also affects the WGS reaction rate on FeMn core catalyst. Therefore, accelerating the diffusion of H_2O through the HZSM-5 shell is beneficial to decrease the WGS reaction. Herein, FeMn@HZSM-5 capsule catalysts using HZSM-5 with Si/Al ratio varying from 25 to 200 as shell were tested in FTO reaction at the same conditions to investigate the influence of Si/Al ratio (hydrophobicity) of zeolite shell on the catalytic performance of capsule catalysts. As shown in Fig. 9, a rather good correlation between product selectivity and Si/Al ratio appears where CO_2 selectivity decreases and the hydrocarbon selectivity increases gradually with the increasing Si/Al ratio. Increasing the Si/Al ratio can increase the hydrophobicity of zeolite, which decreases the adsorption ability of H_2O in zeolite. Therefore, the produced H_2O on FeMn core catalyst can diffuse out of zeolite shell with high Si/Al ratio more quickly than zeolite shell with low Si/Al ratio. Therefore, FeMn@HZSM-5 capsule catalyst using HZSM-5 with high Si/Al ratio (200) can suppress the WGS reaction more effectively, and obtain higher hydrocarbon selectivity and lower CO_2 selectivity.

The proposed reaction mechanism of the FeMn@HZSM-5 capsule catalyst influencing the WGS reaction in FTO is shown in Fig. 10. In FTO

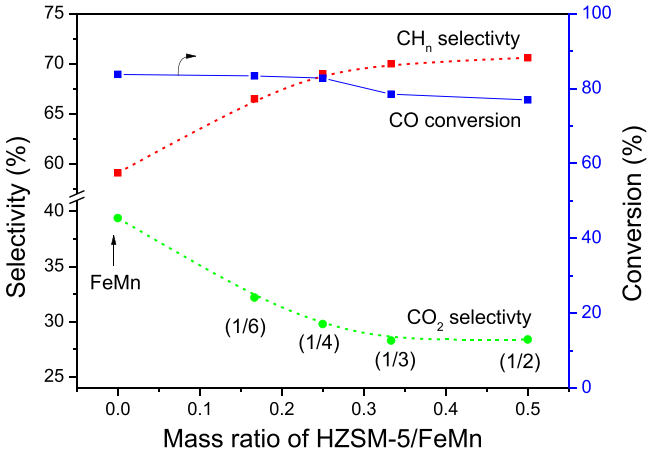

Fig. 8. The effect of HZSM-5/FeMn mass ratio of FeMn@HZSM-5 capsule catalysts on the catalytic performance.

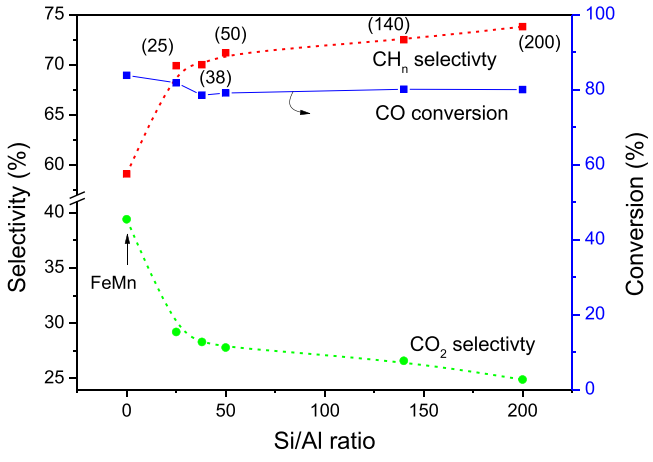

Fig. 9. The effect of Si/Al ratios of zeolite shell on the catalytic performance.

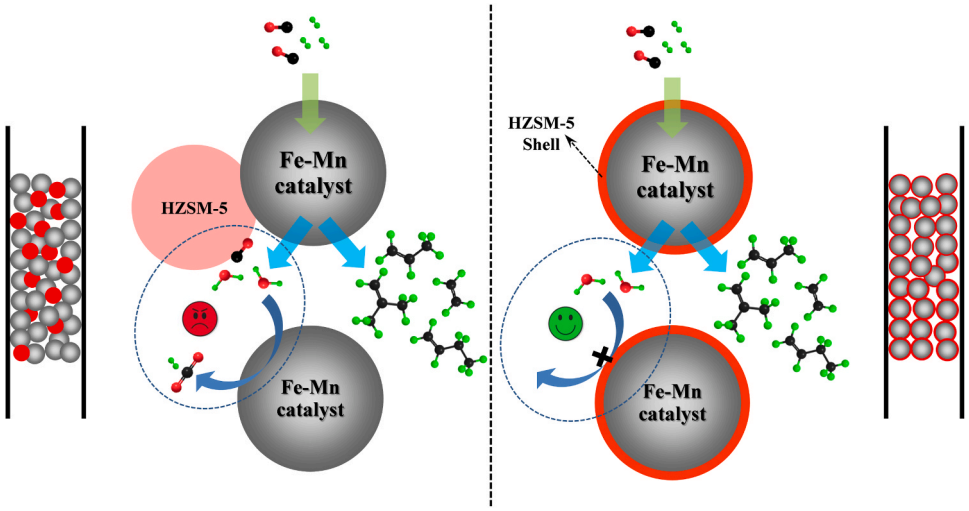

Fig. 10. The proposed action mechanism of the FeMn@HZSM-5 capsule catalyst influencing the WGS reaction in FTO.

reaction, diffusion of the produced H_2O at Fe active sites is a key factor for WGS reaction. For bare FeMn catalyst and its physical mixture catalysts, the produced water from FTO reaction could readily contact with other Fe active site during the diffusion process, which increases the chance of the WGS reaction and accelerates the CO_2 formation. However, the FeMn@HZSM-5 capsule catalyst with the core-shell structure can affect the diffusion of H_2O to FeMn core catalyst. Due to the coverage of HZSM-5 zeolite membrane, the water from one capsule catalyst cannot contact neighboring FeMn cores readily, being free from undergoing further WGS reaction, especially at the cases on high Si/Al ratio zeolite membrane. Therefore, appropriately increased thickness of zeolite shell is beneficial to hinder the H_2O diffusion through shell into core and consequently reduce the chance of WGS reaction. Moreover, zeolite shell with higher Si/Al ratio can promote the diffusion of produced H_2O on FeMn out of the HZSM-5 shell to decrease the WGS reaction. Therefore, among these catalysts, only the FeMn@HZSM-5 capsule catalyst shows the obvious decrease of CO_2 selectivity.

4. Conclusions

In this work, FeMn catalyst and its hybrid catalysts with different structure were tested in FTO reaction. The FeMn@HZSM-5 capsule catalyst with FeMn catalyst as core and HZSM-5 zeolite as shell exhibited better catalytic performance than bare FeMn catalyst and other hybrid catalysts by physically mixing FeMn and HZSM-5 in varied ways. Randomly adding HZSM-5 could not improve the catalytic performance, and the improved performance of FeMn@HZSM-5 capsule catalyst could be attributed to its special core-shell structure as well as confined reaction environment. The special core-shell structure of FeMn@HZSM-5 hindered the diffusion of H_2O into the core and suppressed the WGS reaction effectively. Consequently, on FeMn@HZSM-5 catalyst, the CO_2 formation was depressed and the hydrocarbon selectivity increased obviously, in comparison to bare FeMn catalyst and other hybrid catalysts. This study discovered the new function of capsule catalyst in suppressing the WGS reaction in FTO reaction, lowering CO_2 emission and the finding could help to develop the optimized catalyst for FTO reaction.

CRediT authorship contribution statement

Faen Song: Methodology, Investigation, Validation, Formal analysis, Data curation, Writing – original draft. **Xiaojing Yong:** Funding acquisition, Investigation, Methodology. **Xuemei Wu:** Methodology, Investigation, Formal analysis, Validation. **Wei Zhang:** Investigation, Funding acquisition. **Qingxiang Ma:** Resources, Investigation, Funding acquisition. **Tiejian Zhao:** Investigation, Funding acquisition, **Minghui Tan:** Methodology, Investigation, Visualization, Validation, Writing – original draft, Writing – review & editing, **Zhongshan Guo:** Funding acquisition, Investigation. **Heng Zhao:** Methodology, Investigation. **Guohui Yang:** Conceptualization, Investigation, Supervision, Writing – review & editing. **Noritatsu Tsubaki:** Investigation, Supervision, Writing – review & editing. **Yisheng Tan:** Investigation, Supervision, Project administration, Writing – review & editing.

Declaration of Competing Interest

The authors declare that they have no known competing financial interests or personal relationships that could have appeared to influence the work reported in this paper.

Acknowledgments

This work was financially supported by the National Natural Science Foundation of China (21802155, 21908235 and 21978312), the Key Research Program of Frontier Sciences, Chinese Academy of Sciences (Grant No. QYZDB-SSW-JSC043), International Partnership Program of Chinese Academy of Sciences (Grant No. 122214KYSB20170007), Ningxia Hui Autonomous Region Key R&D Program (Grant No. 2019BFH02016), and Foundation of State Key Laboratory of High-efficiency Utilization of Coal and Green Chemical Engineering (Grant No. 2019-KF-05). Research Project Supported by Shanxi Scholarship Council of China and Fund Program for the Scientific Activities of Selected Returned Overseas Professionals in Shanxi Province are also greatly appreciated.

Appendix A. Supporting information

Supplementary data associated with this article can be found in the online version at doi:10.1016/j.apcatb.2021.120713.

References

[1] N. Rahimi, R. Karimzadeh, Catalytic cracking of hydrocarbons over modified ZSM-5 zeolites to produce light olefins: a review, Appl. Catal. A – Gen. 398 (2011) 1–17.
[2] F. Jiao, J. Li, X. Pan, J. Xiao, H. Li, H. Ma, M. Wei, Y. Pan, Z. Zhou, M. Li, S. Miao, J. Li, Y. Zhu, D. Xiao, T. He, J. Yang, F. Qi, Q. Fu, X. Bao, Selective conversion of syngas to light olefins, Science 351 (2016) 1065–1068.
[3] P. Zhai, C. Xu, R. Gao, X. Liu, M. Li, W. Li, X. Fu, C. Jia, J. Xie, M. Zhao, X. Wang, Y.-W. Li, Q. Zhang, X.-D. Wen, D. Ma, Highly tunable selectivity for syngas-derived alkenes over zinc and sodium-modulated Fe_5C_2 catalyst, Angew. Chem. Int. Ed. 55 (2016) 9902–9907.

[4] H.M. Torres Galvis, J.H. Bitter, C.B. Khare, M. Ruitenbeek, A.I. Dugulan, K.P. de Jong, Supported iron nanoparticles as catalysts for sustainable production of lower olefins, Science 335 (2012) 835–838.

[5] K. Cheng, B. Gu, X. Liu, J. Kang, Q. Zhang, Y. Wang, Direct and highly selective conversion of synthesis gas into lower olefins: design of a bifunctional catalyst combining methanol synthesis and carbon–carbon coupling, Angew. Chem. Int. Ed. 55 (2016) 4725–4728.

[6] L. Zhong, F. Yu, Y. An, Y. Zhao, Y. Sun, Z. Li, T. Lin, Y. Lin, X. Qi, Y. Dai, L. Gu, J. Hu, S. Jin, Q. Shen, H. Wang, Cobalt carbide nanoprisms for direct production of lower olefins from syngas, Nature 538 (2016) 84–87.

[7] X. Wu, S. Xu, W. Zhang, J. Huang, J. Li, B. Yu, Y. Wei, Z. Liu, Direct mechanism of the first carbon–carbon bond formation in the methanol-to-hydrocarbons process, Angew. Chem. Int. Ed. 56 (2017) 9039–9043.

[8] Y. Chen, K. Gong, F. Jiao, X. Pan, G. Hou, R. Si, X. Bao, C–C bond formation in syngas conversion over zinc sites grafted on ZSM-5 zeolite, Angew. Chem. Int. Ed. 59 (2020) 6529–6534.

[9] X. Liu, W. Zhou, Y. Yang, K. Cheng, J. Kang, L. Zhang, G. Zhang, X. Min, Q. Zhang, Y. Wang, Design of efficient bifunctional catalysts for direct conversion of syngas into lower olefins via methanol/dimethyl ether intermediates, Chem. Sci. 9 (2018) 4708–4718.

[10] Y. Xue, J. Li, P. Wang, X. Cui, H. Zheng, Y. Niu, M. Dong, Z. Qin, J. Wang, W. Fan, Regulating Al distribution of ZSM-5 by Sn incorporation for improving catalytic properties in methanol to olefins, Appl. Catal. B: Environ. 280 (2021), 119391.

[11] H.M. Torres Galvis, K.P. de Jong, Catalysts for production of lower olefins from synthesis gas: a review, ACS Catal. 3 (2013) 2130–2149.

[12] Y. Liu, J.-F. Chen, J. Bao, Y. Zhang, Manganese-modified Fe_3O_4 microsphere catalyst with effective zctive phase of forming light olefins from syngas, ACS Catal. 5 (2015) 3905–3909.

[13] Y. Liu, F. Lu, Y. Tang, M. Liu, F.F. Tao, Y. Zhang, Effects of initial crystal structure of Fe_2O_3 and Mn promoter on effective active phase for syngas to light olefins, Appl. Catal. B: Environ. 261 (2020), 118219.

[14] J. Wang, Y. Xu, G. Ma, J. Lin, H. Wang, C. Zhang, M. Ding, Directly converting syngas to linear α-olefins over core–shell Fe_3O_4@MnO_2 catalysts, ACS Appl. Mater. Interfaces 10 (2018) 43578–43587.

[15] X. Fang, B. Liu, K. Cao, P. Yang, Q. Zhao, F. Jiang, Y. Xu, R. Chen, X. Liu, Particle-size-dependent methane selectivity evolution in cobalt-based Fischer–Tropsch synthesis, ACS Catal. 10 (2020) 2799–2816.

[16] T. Lin, K. Gong, C. Wang, Y. An, X. Wang, X. Qi, S. Li, Y. Lu, L. Zhong, Y. Sun, Fischer–Tropsch synthesis to olefins: catalytic performance and structure evolution of Co_2C-based catalysts under a CO_2 environment, ACS Catal. 9 (2019) 9554–9567.

[17] B. Liu, W. Li, Y. Xu, Q. Lin, F. Jiang, X. Liu, Insight into the intrinsic active site for selective production of light olefins in cobalt-catalyzed Fischer–Tropsch synthesis, ACS Catal. 9 (2019) 7073–7089.

[18] C. López, A. Corma, Supported iron nanoparticles as catalysts for sustainable production of lower olefins, ChemCatChem 4 (2012) 751–752.

[19] Z. Li, L. Zhong, F. Yu, Y. An, Y. Dai, Y. Yang, T. Lin, S. Li, H. Wang, P. Gao, Y. Sun, M. He, Effects of sodium on the catalytic performance of CoMn catalysts for Fischer–Tropsch to olefin reactions, ACS Catal. 7 (2017) 3622–3631.

[20] H.M. Torres Galvis, J.H. Bitter, T. Davidian, M. Ruitenbeek, A.I. Dugulan, K.P. de Jong, Iron particle size effects for direct production of lower olefins from synthesis gas, J. Am. Chem. Soc. 134 (2012) 16207–16215.

[21] X.Q. Chen, D.H. Deng, X.L. Pan, Y.F. Hu, X.H. Bao, N-doped graphene as an electron donor of iron catalysts for CO hydrogenation to light olefins, Chem. Commun. 51 (2015) 217–220.

[22] X.-P. Fu, W.-Z. Yu, C. Ma, J. Lin, S.-Q. Sun, S.-Q. Li, P.-N. Ren, F.-Y. Jia, M.-Y. Li, W.-W. Wang, X. Wang, C.-J. Jia, K. Wu, R. Si, C.-H. Yan, Supported Fe_2C catalysts originated from Fe_2N phase and active for Fischer-Tropsch synthesis, Appl. Catal. B: Environ. 284 (2021), 119702.

[23] Y. Chen, X. Li, J. Zhang, N. Zhao, L. Dai, X. Jiang, C. Liu, S. Lyu, Z. Li, Preparation of SiO_2 immobilized Co-based catalysts from ZIF-67 and the enhancement effect for Fischer-Tropsch synthesis, Appl. Catal. B: Environ. 289 (2021), 120027.

[24] Y. Wang, S. Kazumi, W. Gao, X. Gao, H. Li, X. Guo, Y. Yoneyama, G. Yang, N. Tsubaki, Direct conversion of CO_2 to aromatics with high yield via a modified Fischer-Tropsch synthesis pathway, Appl. Catal. B: Environ. 269 (2020), 118792.

[25] V.V. Ordomsky, Y. Luo, B. Gu, A. Carvalho, P.A. Chernavskii, K. Cheng, A. Y. Khodakov, Soldering of iron catalysts for direct synthesis of light olefins from syngas under mild reaction conditions, ACS Catal. 7 (2017) 6445–6452.

[26] Y. Liu, B.-T. Teng, X.-H. Guo, Y. Li, J. Chang, L. Tian, X. Hao, Y. Wang, H.-W. Xiang, Y.-Y. Xu, Y.-W. Li, Effect of reaction conditions on the catalytic performance of Fe-Mn catalyst for Fischer-Tropsch synthesis, J. Mol. Catal. A: Chem. 272 (2007) 182–190.

[27] B. Hu, S. Frueh, H.F. Garces, L. Zhang, M. Aindow, C. Brooks, E. Kreidler, S.L. Suib, Selective hydrogenation of CO_2 and CO to useful light olefins over octahedral molecular sieve manganese oxide supported iron catalysts, Appl. Catal. B-Environ. 132–133 (2013) 54–61.

[28] Z.X. Ma, C.L. Zhou, D.M. Wang, Y.X. Wang, W.X. He, Y.S. Tan, Q.S. Liu, Co-precipitated Fe-Zr catalysts for the Fischer-Tropsch synthesis of lower olefins (C_2–$C_4^=$): Synergistic effects of Fe and Zr, J. Catal. 378 (2019) 209–219.

[29] A.J. Barrios, B. Gu, Y. Luo, D.V. Peron, P.A. Chernavskii, M. Virginie, R. Wojcieszak, J.W. Thybaut, V.V. Ordomsky, A.Y. Khodakov, Identification of efficient promoters and selectivity trends in high temperature Fischer-Tropsch synthesis over supported iron catalysts, Appl. Catal. B: Environ. 273 (2020), 119028.

[30] S. Wang, P. Wang, D. Shi, S. He, L. Zhang, W. Yan, Z. Qin, J. Li, M. Dong, J. Wang, U. Olsbye, W. Fan, Direct conversion of syngas into light olefins with low CO_2 emission, ACS Catal. 10 (2020) 2046–2059.

[31] Y. Cheng, J. Lin, K. Xu, H. Wang, X. Yao, Y. Pei, S. Yan, M. Qiao, B. Zong, Fischer–Tropsch synthesis to lower olefins over potassium-promoted reduced graphene oxide supported iron catalysts, ACS Catal. 6 (2016) 389–399.

[32] X. Yu, J. Zhang, X. Wang, Q. Ma, X. Gao, H. Xia, X. Lai, S. Fan, T. Zhao, Fischer-Tropsch synthesis over methyl modified Fe_2O_3@SiO_2 catalysts with low CO_2 selectivity, Appl. Catal. B-Environ. 232 (2018) 420–428.

[33] T. Li, Y. Yang, C. Zhang, X. An, H. Wan, Z. Tao, H. Xiang, Y. Li, F. Yi, B. Xu, Effect of manganese on an iron-based Fischer–Tropsch synthesis catalyst prepared from ferrous sulfate, Fuel 86 (2007) 921–928.

[34] B. Shi, Z. Zhang, Y. Liu, J. Su, X. Liu, X. Li, J. Wang, M. Zhu, Z. Yang, J. Xu, Y.-F. Han, Promotional effect of Mn-doping on the structure and performance of spinel ferrite microspheres for CO hydrogenation, J. Catal. 381 (2020) 150–162.

[35] Z. Zhang, W. Dai, X.-C. Xu, J. Zhang, B. Shi, J. Xu, W. Tu, Y.-F. Han, MnO_x promotional effects on olefins synthesis directly from syngas over bimetallic Fe-MnO_x/SiO_2 catalysts, AlChE J. 63 (2017) 4451–4464.

[36] Y. Xu, X. Jia, X. Liu, Supported Fe/MnO_x catalyst with Ag doping for remarkably enhanced catalytic activity in Fischer–Tropsch synthesis, Catal. Sci. Technol. 8 (2018) 1953–1970.

[37] Z. Yang, Z. Zhang, Y. Liu, X. Ding, J. Zhang, J. Xu, Y. Han, Tuning direct CO hydrogenation reaction over Fe-Mn bimetallic catalysts toward light olefins: effects of Mn promotion, Appl. Catal. B: Environ. 285 (2021), 119815.

[38] H.M. Torres Galvis, A.C.J. Koeken, J.H. Bitter, T. Davidian, M. Ruitenbeek, A. I. Dugulan, K.P. de Jong, Effects of sodium and sulfur on catalytic performance of supported iron catalysts for the Fischer–Tropsch synthesis of lower olefins, J. Catal. 303 (2013) 22–30.

[39] X. Zhou, J. Ji, D. Wang, X. Duan, G. Qian, D. Chen, X. Zhou, Hierarchical structured α-Al_2O_3 supported S-promoted Fe catalysts for direct conversion of syngas to lower olefins, Chem. Commun. 51 (2015) 8853–8856.

[40] N. Lohitharn, J.G. Goodwin, Effect of K promotion of Fe and FeMn Fischer–Tropsch synthesis catalysts: analysis at the site level using SSITKA, J. Catal. 260 (2008) 7–16.

[41] Z. Zhao, W. Lu, R. Yang, H. Zhu, W. Dong, F. Sun, Z. Jiang, Y. Lyu, T. Liu, H. Du, Y. Ding, Insight into the formation of Co@Co_2C catalysts for direct synthesis of higher alcohols and olefins from syngas, ACS Catal. 8 (2017) 228–241.

[42] W. Gong, R.-P. Ye, J. Ding, T. Wang, X. Shi, C.K. Russell, J. Tang, E.G. Eddings, Y. Zhang, M. Fan, Effect of copper on highly effective Fe-Mn based catalysts during production of light olefins via Fischer-Tropsch process with low CO_2 emission, Appl. Catal. B: Environ. 278 (2020), 119302.

[43] J. Bao, J. He, Y. Zhang, Y. Yoneyama, N. Tsubaki, A core/shell catalyst produces a spatially confined effect and shape selectivity in a consecutive reaction, Angew. Chem. Int. Ed. 47 (2008) 353–356.

[44] Q.H. Lin, G.H. Yang, Q.J. Chen, R.G. Fan, Y. Yoneyama, H.L. Wan, N. Tsubaki, Design of a hierarchical meso/macroporous zeolite-supported cobalt catalyst for the enhanced direct synthesis of isoparaffins from syngas, ChemCatChem 7 (2015) 682–689.

[45] Q.H. Lin, Q.D. Zhang, G.H. Yang, Q.J. Chen, J. Li, Q.H. Wei, Y.S. Tan, H.L. Wan, N. Tsubaki, Insights into the promotional roles of palladium in structure and performance of cobalt-based zeolite capsule catalyst for direct synthesis of C_5-C_{11} iso-paraffins from syngas, J. Catal. 344 (2016) 378–388.

[46] G.H. Yang, C. Xing, W. Hirohama, Y.Z. Jin, C.Y. Zeng, Y. Suehiro, T.J. Wang, Y. Yoneyama, N. Tsubaki, Tandem catalytic synthesis of light isoparaffin from syngas via Fischer-Tropsch synthesis by newly developed core-shell-like zeolite capsule catalysts, Catal. Today 215 (2013) 29–35.

[47] C. Zhu, D.P. Gamliel, J.A. Valla, G.M. Bollas, Fischer-tropsch synthesis in monolith catalysts coated with hierarchical ZSM-5, Appl. Catal. B: Environ. 284 (2021), 119719.

[48] G.H. Yang, D. Wang, Y. Yoneyama, Y.S. Tan, N. Tsubaki, Facile synthesis of H-type zeolite shell on a silica substrate for tandem catalysis, Chem. Commun. 48 (2012) 1263–1265.

[49] G. Yang, N. Tsubaki, J. Shamoto, Y. Yoneyama, Y. Zhang, Confinement effect and synergistic function of H-ZSM-5/Cu-ZnO-Al_2O_3 capsule catalyst for one-step controlled synthesis, J. Am. Chem. Soc. 132 (2010) 8129–8136.

[50] L. Tan, F. Wang, P. Zhang, Y. Suzuki, Y. Wu, J. Chen, G. Yang, N. Tsubaki, Design of a core–shell catalyst: an effective strategy for suppressing side reactions in syngas for direct selective conversion to light olefins, Chem. Sci. 11 (2020) 4097–4105.